Synthetic and Systems Biotechnology 9 (2024) 684–693

Contents lists available at ScienceDirect

Synthetic and Systems Biotechnology

journal homepage: www.keaipublishing.com/en/journals/synthetic-and-systems-biotechnology

Original Research Article

New *N*-acylated aminoalkanoic acids from tea roots derived biocontrol agent *Clonostachys rosea* 15020

Jiaming Yu [a], Yue Zhang [b], Li Zhang [b], Jie Shi [a], Kun Wang [a], Weize Yuan [a], Zexu Lin [a], Shangqian Ning [a], Bohao Wang [a], Xinye Wang [a], Yuyang Qiu [c], Tom Hsiang [d], Lixin Zhang [a], Xueting Liu [a], Guoliang Zhu [a,*]

[a] State Key Laboratory of Bioreactor Engineering, East China University of Science and Technology, Shanghai 200237, China
[b] Department of Chemistry, Boston University, Boston, MA, USA
[c] School of Insurance, Shandong University of Finance and Economics, Jinan, 250014, China
[d] School of Environmental Sciences, University of Guelph, Guelph, Ontario, N1G 2W1, Canada

ARTICLE INFO

Keywords:
Endophytic fungi
N-acylated aminoalkanoic acid
FBMN
Adenylate-forming enzyme

ABSTRACT

Four new *N*-acylated aminoalkanoic acids, namely clonoroseins E–H (**1**–**4**), together with three previously identified analogs, clonoroseins A, B, and D (**5**–**7**), were identified from the endophytic fungus *Clonostachys rosea* strain 15020 (CR15020), using Feature-based Molecular Networking (FBMN). The elucidation of their chemical structures, including their absolute configurations, was achieved through spectroscopic analysis combined with quantum chemical calculations. Bioinformatics analyses suggested that an iterative type I HR-PKS (CrsE) generates the polyketide side chain of these clonoroseins. Furthermore, a downstream adenylate-forming enzyme of the PKS (CrsD) was suspected to function as an amide synthetase. CrsD potentially facilitates the transformation of the polyketide moiety into an acyl-AMP intermediate, followed by nucleophilic substitution with either β-alanine or γ-aminobutyric acid to produce amide derivatives. These findings significantly expand our understanding of PKS-related products originating from *C. rosea* and also underscore the powerful application of FBMN analytical methods in characterization of new compounds.

1. Introduction

Natural products (NPs) continue to serve as valuable sources for drug development. Nearly 50 % of newly approved drugs within the last 40 years have their origins in secondary metabolites produced by various organism [1]. Among these organisms, plant endophytic fungi, particularly those engaged in interactions with plant pathogens, have more recently garnered attention due to their production of diverse NPs that are often endowed with significant bioactivity [2,3]. One such noteworthy organism is the ascomycete fungus *Clonostachys rosea.* It is a mycoparasite, possessing biocontrol capabilities against various fungal phytopathogen, nematodes, and insects [4]. This ability can be partially attributed to its secretion of cell-wall-degrading enzymes, including chitinases, glucanases, and proteases. Additionally, *C. rosea* is known to activate defense enzymes and genes related to defense in plants [5,6].

Recent genome sequencing of *C. rosea* isolates 67-1, and IK726 has unveiled substantial biosynthetic capabilities, particularly in the production of various classes of secondary metabolites, notably polyketides (31 PKS genes) and non-ribosomal peptides (17 NRPS genes) [7,8]. These genes potentially encode a broad spectrum of antibiotics or toxins, which likely contribute to the biocontrol efficacy of *C. rosea* during competitive interactions with other fungi [6]. Gliocladines A–E and several antinematodal secondary metabolites have been identified from *C. rosea* 1A [9]. Additionally, bisorbicillinoids, clonorosein A, and TMC-151C&E were discovered in *C. rosea* YRS-06, albeit with weak antimicrobial activity. Notably, *C. rosea* has also yielded compounds like bionectin B, verticillin D, and heptapeptide cyclo-(-Gly-Leu-Ile-Val-Val-Trp-β-Ala), which exhibit significant cytotoxic activity [10,11]. Among these natural products, only a few are polyketides, a stark contrast to the substantial repertoire of PKS gene content within its genome [7,8], suggesting significant potential of unexplored natural products. The unlocking of these untapped

Peer review under responsibility of KeAi Communications Co., Ltd.
* Corresponding author.
E-mail address: zhuguoliang@ecust.edu.cn (G. Zhu).

https://doi.org/10.1016/j.synbio.2024.05.006
Received 29 March 2024; Received in revised form 30 April 2024; Accepted 9 May 2024
Available online 11 May 2024

biosynthetic pathways may expand the profile of bioactive natural products in *C. rosea*.

The discovery of these potential natural products requires the application of rapid and highly sensitive analytical techniques. Advancements in LC-MS/MS techniques have paved the way for the development of molecular networking (MN), equipping researchers with powerful analytical tools in natural product dereplication and targeted isolation. In a recent study, MN was effectively employed to characterize trace amount of biosynthetic intermediates of epicospirocin [12]. To enhance the capabilities of MN, Feature-based molecular networking (FBMN) was developed and became widely accessible in 2020 [13]. In comparison to the traditional MN approach, the FBMN integrates the output of chromatographic feature detection with alignment tools. This integration results in more concise and legible networks, capable of distinguishing isomers, which is especially valuable [13]. The FBMN approach was instrumental in proper annotation of five known and eleven previously unidentified *N*-Acyl-L-homoserine lactones [14]. Furthermore, FBMN-based analysis unveiled that teadenol A and fuzhuanin A were derived from epigallocatechin gallate after exposure to an endophytic fungus found from tea leaves [15].

In order to probe the chemical diversity of *C. rosea* CR15020 when cultivated in a rice medium, the current study was conducted. Guided by FBMN analysis, a series of potential new analogs related to the antifungal clonoroseins [6] were identified within the network and subsequently confirmed through UV, HRMS and NMR data. Targeted isolation efforts led to the characterization of seven *N*-acylated aminoalkanoic acids, including four newly discovered compounds named clonoroseins E−H (**1**−**4**), as well as the previously reported clonoroseins A, B, and D (**5**−**7**). The structures of these compounds were fully interpreted through comprehensive spectrographic analysis and computational methods.

2. Materials and methods

2.1. Microbial strain culture, identification, and genome sequencing

Plant endophytic fungal strain *C. rosea* 15020 was originally isolated from tea roots in Canada. This strain has been preserved in the China General Microbiological Culture Collection Centre (accession no. CGMCC21037), member of World Data Centre for Microorganisms (WDCM 550), and has been stored at −80 °C. Potato dextrose agar (PDA) was targeted to culture the strain for laboratory experiments. The DNA of *C. rosea* 15020 was extracted with CTAB (cetyltrimethylammonium bromide) as earlier reported [16]. ITS of *C. rosea* 15020 ribosomal DNA analyses with sequences from related species using CLUSTAL W [17] after DNA was amplified with Primers (F: TCCTCCGCTTATTGATATGC, R: GGAAGTAAAAGTCGTAACAAGG.) A phylogenetic tree was constructed using the neighbour-joining method [18] with MEGA 7.0 [19]. Bootstrap replications (1000) were used to establish brance support. The ITS ribosomal DNA sequences (accession no. MW600462) and the presumed clonorosein gene cluster (accession no. ON817174) of *C. rosea* 15020 have been deposited in GenBank. Genomic sequencing and assembly of strain *C. rosea* 15020 was performed using the same method as previously described [10].

2.2. Fermentation, extraction, and isolation

Fermentation and extraction. Strain *C. rosea* 15020 was cultured on PDA at 28 °C for 10 days, and agar plugs (5-mm-diameter) were transferred to 250 mL Erlenmeyer flasks containing 100 mL of potato dextrose broth (PDB). The flasks were incubated at 28 °C, on a rotary shaker, at 200 rpm for 5 days to create the seed culture. Then, 3 mL of the culture was placed into each of 125 bags containing 80 g of autoclaved rice and 120 mL of distilled H_2O. These inoculum bags were incubated at 28 °C for 35 days. After that, 10 kg of whole cultures were extracted with EtOAc (3 × 20 L) and concentrated under reduced pressure to yield a dark brown gum (13 g).

*Isolation process for compounds **1**–**7***. The crude extract was dissolved in methanol and subjected to Sephadex LH-20 elution with 100 % MeOH to yield fifteen fractions (N1–N15). Fraction N5 (472.9 mg) was subjected to ODS-MPLC with an ACN-H_2O gradient (10%–100 %) elution for 60 min to get eight sub-fractions (F1–F8). Sub-fraction F3 (58.7 mg) was further purified by semipreparative HPLC (Cosmosil Cholester, 10 × 250 mm, 4 mL/min, 35 % acetonitrile and 65 % aqueous solution) to obtain compounds **1** (0.6 mg, t_R = 12.5 min) and **2** (1.9 mg, t_R = 14.5 min). Fraction F4 (113.0 mg) was further purified by semipreparative HPLC (Cosmosil Cholester, 4 mL/min, 10 × 250 mm, 40 % acetonitrile and 60 % aqueous solution isocratic elution) to obtain compound **3** (0.6 mg, t_R = 25.9 min), **4** (1.1 mg, t_R = 19.5 min), **5** (20.3 mg, t_R = 16.7 min), **6** (9.7 mg, t_R = 19.0 min) and **7** (2.0 mg, t_R = 17.6 min) (Fig. S9).

Clonorosein E (**1**): transparent oil; $[\alpha]_D^{24.0}$ = +31.7 (*c* 0.06, MeOH); UV (MeOH) λ_{max} (log ε) 213 (3.85) nm; CD (0.5 μM, MeOH) λ_{max} ($\Delta\varepsilon$) 220 (+1.33) nm; ^{1}H NMR and ^{13}C NMR data, see Table 2; HR-ESI-MS: *calcd.* For $C_{12}H_{22}NO_3$ $[M + H]^+$: 228.1594, found: 228.1596.

Clonorosein F (**2**): transparent oil; $[\alpha]_D^{24.0}$ = +50.0 (*c* 0.19, MeOH); UV (MeOH) λ_{max} (log ε) 213 (4.10) nm; CD (0.5 μM, MeOH) λ_{max} ($\Delta\varepsilon$) 220 (+1.18) nm; ^{1}H NMR and ^{13}C NMR data, see Table 2; HR-ESI-MS: *calcd.* For $C_{13}H_{24}NO_3$ $[M + H]^+$: 242.1751, found: 242.1756.

Clonorosein G (**3**): transparent oil; $[\alpha]_D^{24.0}$ = +31.7 (*c* 0.06, MeOH); UV (MeOH) λ_{max} (log ε) 195 (4.05) nm; CD (0.5 μM, MeOH) λ_{max} ($\Delta\varepsilon$) 205 (+1.09), 220 (1.21) nm; ^{1}H NMR and ^{13}C NMR data, see Table 2; HR-ESI-MS: *calcd.* For $C_{16}H_{32}NO_3$ $[M + H]^+$: 286.2368, found: 286.2373.

Clonorosein H (**4**): transparent oil; $[\alpha]_D^{24.0}$ = +36.4 (*c* 0.11, MeOH); UV (MeOH) λ_{max} (log ε) 213 (4.15) nm; CD (0.5 μM, MeOH) λ_{max} ($\Delta\varepsilon$) 225 (+6.06) nm; ^{1}H NMR and ^{13}C NMR data, see Table 2; HR-ESI-MS: *calcd.* For $C_{15}H_{28}NO_3$ $[M + H]^+$: 270.2056, found: 270.2062.

Clonorosein D (**7**): transparent oil; $[\alpha]_D^{24.0}$ = +20.5 (*c* 0.20, MeOH); UV (MeOH) λ_{max} (log ε) 195 (4.20) nm; CD (0.5 μM, MeOH) λ_{max} ($\Delta\varepsilon$) 210 (+1.10) nm; ^{1}H NMR and ^{13}C NMR data, see Table S1; HR-ESI-MS: *calcd.* For $C_{15}H_{28}NO_3$ $[M + H]^+$: 272.2212, found: 272.2217.

2.3. Theory and calculation details

The Quantum chemical calculations were carried out using density functional theory (DFT) in Gaussian 09 [20]. Initial conformation search was executed using Sybyl-X 2.0, followed by geometry optimization using the SCRF/PCM method at the B3LYP/6-31G(d) level [21]. TDDFT was used to calculate the electronic excitation energies and rotational strengths at B3LYP/6-31+G(d) in methanol solution [22].

2.4. Antimicrobial and antifungal assay

Antimicrobial experiments were conducted following CLSI guidelines [23] in growth inhibition tests.

3. Results

3.1. Characterization and identification of the strain CR15020

After incubation on a PDA agar plate at 28 °C for 7 days, the strain CR15020 formed grayish-white to yellowish-white colonies (Fig. 1A) and was identified as *Clonostachys rosea* by morphological [24] and ITS ribosomal DNA analyses. The organism shares 99 % similarity with *C. rosea* CBS 128894 (accession number: MH865144) (Fig. 1B).

3.2. LC-MS/MS and FBMN guided the discovery of new clonoroseins

Eleven media (Rice, Maya, Z5, Q6, Z2, ISP2, Z4, CS, SWS, MM, and YPD) were used in the fermentation to compare the chemical diversity of CR15020 extracts. The crude extract from the culture in rice medium showed the highest metabolic chemical diversity according to the HPLC

Table 1
Annotation for 41 nodes in the clonorosein cluster I from the CR15020 Featured Based Molecular Networking.

Node (Observed precursor *m/z*)	Molecular formula $[M+H]^+$	Calc. *m/z*	[a]Δ (ppm)	$\Delta_{m/z}$ from seed clonorosein B (6)	Annotation
165.1275	–	–	–	–	–
167.1431	–	–	–	–	–
167.1431	–	–	–	–	–
174.1125	$C_8H_{16}O_3N$	174.1130	2.9	−96.0938	-C_7H_{12} from **6**
174.1491	–	–	–	–	–
183.1384	–	–	–	–	–
188.1281	$C_9H_{18}O_3N$	188.1287	3.2	−82.0782	-C_6H_{10} from **6**
190.1438	$C_9H_{20}O_3N$	190.1443	2.6	−80.0625	-C_6H_8 from **6**
200.1282	$C_{10}H_{18}O_3N$	200.1287	2.5	−70.0781	-C_5H_{10} from **6**
202.1438	$C_{10}H_{20}O_3N$	202.1443	2.5	−68.0625	-C_5H_8 from **6**
206.1544	–	–	–	–	–
216.1599	$C_{11}H_{22}O_3N$	216.1600	0.5	−54.0464	-C_4H_6 from **6**
228.1596	$C_{12}H_{22}O_3N$	228.1600	1.8	−42.0467	clonorosein E (**1**)
230.2478	–	–	–	–	–
232.1549	–	–	–	–	–
234.1853	–	–	–	–	–
236.1650	–	–	–	–	–
242.1756	$C_{13}H_{24}O_3N$	242.1756	0.0	−28.0307	clonorosein F (**2**)
246.1853	–	–	–	–	–
250.1799	–	–	–	–	–
254.1754	$C_{14}H_{24}O_3N$	254.1756	0.8	−16.0309	-CH_4 from **6**
254.1754	$C_{14}H_{24}O_3N$	254.1756	0.8	−16.0309	-CH_4 from **6**
256.1907	$C_{14}H_{26}O_3N$	256.1913	2.3	−14.0156	clonorosein A (**5**)
256.1907	$C_{14}H_{26}O_3N$	256.1913	2.3	−14.0156	isomer of **6**
258.2065	$C_{14}H_{28}O_3N$	258.2069	1.5	−11.9998	-C from **6**
262.1801	–	–	–	–	–
264.1958	–	–	–	–	–
268.1913	$C_{15}H_{26}O_3N$	268.1913	0.0	−2.0150	-H_2 from **6**
268.1913	$C_{15}H_{26}O_3N$	268.1913	0.0	−2.0150	-H_2 from **6**
270.2062	$C_{15}H_{28}O_3N$	270.2069	2.6	−0.0001	clonorosein H (**4**)
270.2063	$C_{15}H_{28}O_3N$	270.2069	2.2	0.0000	clonorosein B (**6**)
272.2217	$C_{15}H_{30}O_3N$	272.2226	3.3	2.0154	clonorosein D (**7**)
274.2015	–	–	–	–	–
274.2737	–	–	–	–	–
282.2062	$C_{16}H_{28}O_3N$	282.2069	2.5	11.9999	+C from **6**
284.2223	$C_{16}H_{30}O_3N$	284.2226	1.1	14.0160	+CH_2 from **6**
286.2016	–	–	–	15.9953	–
286.2373	$C_{16}H_{32}O_3N$	286.2382	3.1	16.0310	Clonorosein G (**3**)
287.2412	–	–	–	–	–
288.2167	–	–	–	–	–
292.1881	$C_{17}H_{26}O_3N$	292.1913	11.0	21.9818	+C_2H_2 from **7**

[a] Δ = (Observed *m/z* – Calc. *m/z*)/Calc. *m/z*; "-" means less possible to be clonorosein anologs.

profile (Fig. S10). *C. rosea* isolate CR15020 was grown using 10 kg of rice medium for 35 days, followed by extraction using ethyl acetate (EA) to obtain 13 g of crude extract, which was subjected to LC-HR-MS analysis (Fig. 2A). A previously reported *N*-acylated aminoalkanoic acid, clonorosein B (**6**) [6], was identified from the chromatogram of CR15020 according to its UV spectrum and HR-MS data from CR15020 EA extract sub-fraction N5 (Fig. 2C and Fig. S7). We carried out feature-based molecular networking (workflow version release_28.2) on the sub-fraction N5 LC-MS/MS dataset to uncover new clonoroseins analogs using clonorosein B (**6**) as the seed (Fig. 2A, Fig. S1), which was subsequently identified to be within a cluster composed of 41 nodes (Fig. 2B). Further careful annotation (Table 1) using their precursor mass alongside HR-ESI-MS data uncovered 22 potential clonorosein nodes, seven of which were also detected from HPLC chromatogram with similar UV spectra with **6** (Fig. 2C). Three of these nodes possessing precursor *m/z* of 256.1907 $[M+H]^+$, 270.2063 $[M+H]^+$, and 272.2217 $[M+H]^+$ that are identical to known compounds clonorosein A/B/D, respectively, and three nodes displayed previously unreported *m/z* of 228.1596, 242.1756, 286.2373. (Table 1).

Guided by the FBMN findings, the clonorosein yield and structure diversity were compared among sub-fractions N1–N15, and N5 was chosen for subsequent purification for new clonorosein analogs. Targeted isolation with the unreported *m/z* was conducted using LC-MS analysis, chromatographic methods, and spectroscopic techniques (Fig. 2C), leading to the identification of four new clonoroseins, known as clonorosein E−H (**1**−**4**), alongside three previously characterized compounds, clonorosein A, B, and D (**5**−**7**). Based on HR-MS, 1D&2D NMR, and ESI-MS/MS analysis (Fig. 3, Fig. S2−S8, Table 2, and Table S1), their structures were fully elucidated. Relative configurations were identified through a comparison of ^{1}H NMR chemical shifts with synthesized analogs, and absolute configurations were determined through quantum chemical ECD computational methods (Fig. 4).

3.3. Structure elucidation of isolated clonoroseins

The molecular formula of **1** was revealed to be $C_{12}H_{21}NO_3$ (228.1588 $[M + H]^+$, calcd. for 228.1594) through HRESIMS (Fig. S2a), implying three degrees of unsaturation. The combined analysis of ^{1}H, ^{13}C, and HSQC spectra of **1** (Table 2, Figs. S2b, S2c, and S2e) revealed 12 carbon resonances, composed of two carbonyl carbons (δ_C 174.7 and 168.4), one olefinic quaternary carbon (δ_C 129.4), one sp^2 methine [δ_C/δ_H 140.6/6.00 (d, J = 9.8 Hz)], one saturated methine (δ_C/δ_H 31.9/2.42), four sp^3 methylenes (δ_C/δ_H 35.7/3.28, 34.8/2.33, 38.9/1.29&1.21, and 20.0/1.21), three methyl groups, including one singlet (δ_C/δ_H 12.7/1.72), one doublet [δ_C/δ_H 20.2/0.92, (d, J = 6.7 Hz)], and one triplet [δ_C/δ_H 14.0/0.84, (d, J = 6.9 Hz)]. The ^{1}H–^{1}H COSY (Fig. 3B and Fig. S2d) of **1** elucidated the existence of two proton spin systems including H-3−H-7 and NH–H-1′−H-2′, according to the crosspeaks between H_3-7/H_2-6, H_2-6/H_2-5, H_2-5/H-4, H-4/H-3, H-4/H_3-9, as well as NH/H_2-1′ and H_2-1′/H_2-2′. Further HMBC correlations of H_2-1′ to C-3′ and H_2-2′ to C-3′ indicated the presence of an N-substituted β-alanine moiety linked to an unsaturated acyl side chain via a 2-methyl-2-enamide group following the major HMBC correlations of H_3-8 to C-1, C-2, C-3 and H_2-1′ to C-1 (Fig. S2f). The $\Delta^{2,3}$ double bond was designated as an *E* configuration based on the observation of crosspeaks between H_3-8/H-4 within the NOESY spectrum (Fig. S2g). To identify the absolute configuration of **1**, the time-dependent density functional theory (TD-DFT)-based electronic circle dichromatography (ECD) calculation of two epimers 4*R*-**1**/4*S*-**1** was performed, resulting in the identification of the 4*S* configuration of **1** (Fig. 4A). Therefore, the structure of **1** was established, shown in Fig. 3A, consisting of a new analog of clonoroseins, named clonorosein E.

The molecular formula of **2** was identified as $C_{13}H_{23}NO_3$ according to the HRESIMS (Fig. S3a) analysis (242.1457 $[M + H]^+$, calcd. for 242.1750), indicating three degrees of unsaturation. The ^{1}H and ^{13}C NMR data of **2** (Table 2, Figs. S3b, S3c, and S3e) exhibited high similarity with those of **1**, aside from a supplemental sp^3 methylene (δ_C/δ_H 25.0/1.89), demonstrating its identity as a homolog of **1**. The presence of an N-substituted γ-aminobutyric acid moiety in **2** was revealed through further analysis of 2D NMR spectra, instead of the β-alanine fragment of **1**, according to the ^{1}H–^{1}H COSY crosspeaks of NH/H_2-1′, H_2-1′/H_2-2′, and H_2-2′/H_2-3′ (Fig. S3d) as well as HMBC correlations of H_2-1′ to C-1, H_2-2′ to C-4, and H_2-3′ to C-4 (Fig. S3f). The $\Delta^{2,3}$ double bond was established as being in the *E* configuration by NOESY correlation of H_3-8/H-4 (Fig. S3g), and the absolute configuration at C-4 was assigned as *S* through ECD calculation (Fig. 4B). Thus, **2** was highlighted as illustrated in Fig. 3A, and identified as clonorosein F.

HRESIMS (Fig. S4a) analysis demonstrated the molecular formula of

Table 2
^{1}H and ^{13}C NMR Data of clonorosein E–H (**1**–**4**).

	clonorosein E (1)		clonorosein F (2)		clonorosein G (3)		clonorosein H (4)	
Pos	δ_H[a] mult (*J* in Hz)	δ_C[b], type	δ_H[c] mult (*J* in Hz)	δ_C[d], type	δ_H[c] mult (*J* in Hz)	δ_C[d], type	δ_H[a] mult (*J* in Hz)	δ_C[b], type
1		168.4, C		170.4, C		178.1, C		168.3, C
1-NH	7.77, t (5.6)		6.12, t (5.4)		5.87, brs		7.73 t (5.5)	
2		129.4, C		128.9, C	2.28, m	39.2, CH		129.1, C
3	6.00, d (9.8)	140.6, CH	6.14, d (10.1)	143.2, CH	1.39, m	41.5, CH_2	5.99, d (9.8)	140.8, CH
					1.34, m			
4	2.42, m	31.9, CH	2.46, m	32.9, CH	1.52, m	27.8, CH	2.53, m	29.9, CH
5a	1.29, m	38.9, CH_2	1.33, m	39.3, CH_2	1.19, m	45.5, CH_2	1.27, m	44.3, CH_2
5b	1.21, m		1.26, m		0.94, m		1.09, m	
6	1.21, m	20.0, CH_2	1.26, m	20.7, CH_2	1.50, m	29.7, CH	1.29, m	29.9, CH
7a	0.84, t (6.9)	14.0, CH_3	0.86, t (7.0)	14.1, CH_3	1.25, m	39.2, CH_2	1.21, m	39.4, CH_2
7b					1.00, m		1.06, m	
8	1.72, s	12.7, CH_3	1.84, s	12.9, CH_3	1.33, m	20.1, CH_2	1.28, m	19.4, CH_2
					1.23, m		1.22, m	
9	0.92, d (6.7)	20.2, CH_3	0.97, d (6.6)	20.3, CH_3	0.87, t (7.2)	14.6, CH_3	0.84, t (7.0)	14.3, CH_3
10					1.10, d (6.8)	17.6, CH_3	1.74, s	12.6, CH_3
11					0.84, d (6.4)	20.3, CH_3	0.92, d (6.7)	20.8, CH_3
12					0.83, d (6.5)	20.2, CH_3	0.79, d (6.5)	19.3, CH_3
1′	3.28, dt (5.6, 6.7)	35.7, CH_2	3.39,	39.3, CH_2	3.32, m	38.9, CH_2	3.28, dt (5.5,7.0)	35.5, CH_2
2′	2.33, t (6.7)	34.8, CH_2	1.89,	25.0, CH_2	1.84, m	25.3, CH_2	2.38, t (7.0)	35.2, CH_2
3′		174.7, C	2.42, t (7.0)	31.9, CH_2	2.38, t (6.2)	31.9, CH_2		173.3, C
4′				177.4, C		177.3, C		

[a] Recorded at 600 MHz in DMSO-d_6.
[b] Recorded at 150 MHz in DMSO-d_6.
[c] Recorded at 600 MHz in $CDCl_3$.
[d] Recorded at 150 MHz in $CDCl_3$.

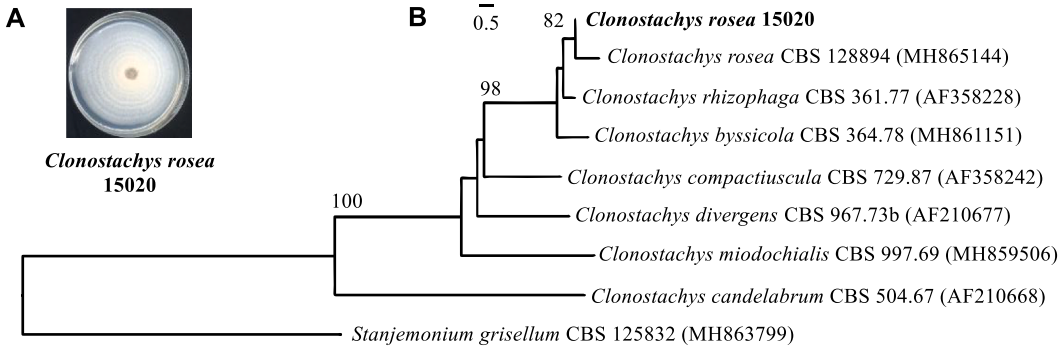

Fig. 1. Morphology and phylogenetic tree of *C. rosea* 15020. (A) Colony characteristics of 15020 grown on potato dextrose agar at 28 °C for 10 days. (B) Neighbour-joining tree of CR15020 based on ITS sequences. Numbers at nodes indicate levels of bootstrap support (%) based on a neighbour-joining analysis of 1000 resampled datasets; only values > 50 % are shown. NCBI accession numbers are provided in parentheses. The bar represents 0.5 nucleotide substitutions per site.

3 to be $C_{16}H_{31}NO_3$ (286.2376 $[M + H]^+$, calcd. for 286.2368), indicating two degrees of unsaturation. According to the combined analysis of ^{1}H, ^{13}C, and HSQC spectra derived from **3** (Table 2, Figs. S4b, S4c, and S4e), 16 carbon resonances were observed, composed of two carbonyl carbons (δ_C 178.1 and 177.3), three saturated methines (δ_C/δ_H 39.2/2.28; 27.8/1.52; 29.7/1.50), seven sp^3 methylenes (δ_C/δ_H 41.5/1.37; 45.5/1.19&0.94; 39.2/1.25&1.00; 20.1/1.33&1.23; 38.9/3.32; 25.3/1.84; 31.9/2.38), and four methyls, including three doublets [δ_C/δ_H 20.3/0.84, (d, $J = 6.4$ Hz); 20.2/0.83, (d, $J = 6.5$ Hz); 17.6/1.10, (d, $J = 6.8$ Hz)], and one triplet [δ_C/δ_H 14.6/0.87, (t, $J = 6.9$ Hz)]. The presence of two proton spin systems was revealed through the ^{1}H–^{1}H COSY (Fig. S4d) conducted on **3**, including H-10–H-2–H-3–[H-4–H-11]–H-5–[H-6–H-12]–H-7–H-8–H-9 and NH–H-1′–H-2′–H-3′. Further HMBC correlations between H_2-1′ to C-1 and H_2-2′ to C-4′ indicated the presence of an N-substituted γ-aminobutyric acid moiety attached to a saturated acyl side chain via an amide group based on the major HMBC correlations of H_3-10 to C-1, C-2, C-3 and H_2-1′ to C-1 (Fig. S4f). The acyl side chain was verified to be 2,4,6-trimethyl-pelargonyl according to the critical HMBC correlations of H_3-10 to C-1/C-2/C-3, H_3-11 to C-3/C-4/C-5, H_3-12 to C-5/C-6/C-7, and H_3-9 to C-8/C-7 (Fig. S4f). The relative configuration between C-2 and C-4 was assigned to be *anti* based on the little difference in chemical shift between the C-3 methylene protons, H-3a and H-3b ($\Delta\delta < 0.1$ ppm), according to the empirical rule outlined by Schmidt and colleagues [25]. C-4 and C-6 were confirmed to be in a *syn* configuration through comparison of the Δδ of H-3a/H-3b and H-5a/H-5b to the synthesized compounds (2*R*,4*S*,6*S*)-*tert*-butyl-2,4,6-trymethyl-8-phenyloctanoate and (2*R*,4*S*,6*R*)-*tert*-butyl-2,4,6-trymethyl-8-phenyloctanoate [25] (Fig. 3C). Further ECD determination of two enantiomers 2*S*,4*R*,6*S*-**3**/2*R*,4*S*,6*R*-**3** was conducted, identifying the 2*S*,4*R*,6*S*- configuration of **3** (Fig. 4C). Therefore, the structure of **3** was defined as shown in Fig. 3A, named clonorosein G.

The molecular formula of **4** was determined to be $C_{15}H_{27}NO_3$ following the HRESIMS (Fig. S5a) analysis (270.2063 $[M + H]^+$, calcd. for 270.2056), suggesting the presence of three degrees of unsaturation. The ^{1}H and ^{13}C NMR data for **4** (Table 2, Figs. S5b, S5c, and S5e) exhibited high similarity to those of **1**, apart from three supplemental saturated carbon resonances in the acyl side chain, one methine (δ_C/δ_H 31.5/1.29), one methylene ($\delta_{C/H}$ 39.4/1.21&1.06), and a methyl doublet [δ_C/δ_H 19.3/0.79, (d, $J = 6.5$ Hz)], indicating its identity as a homolog of **1**. The ^{1}H–^{1}H COSY (Fig. S5d) of **4** uncovered the existence

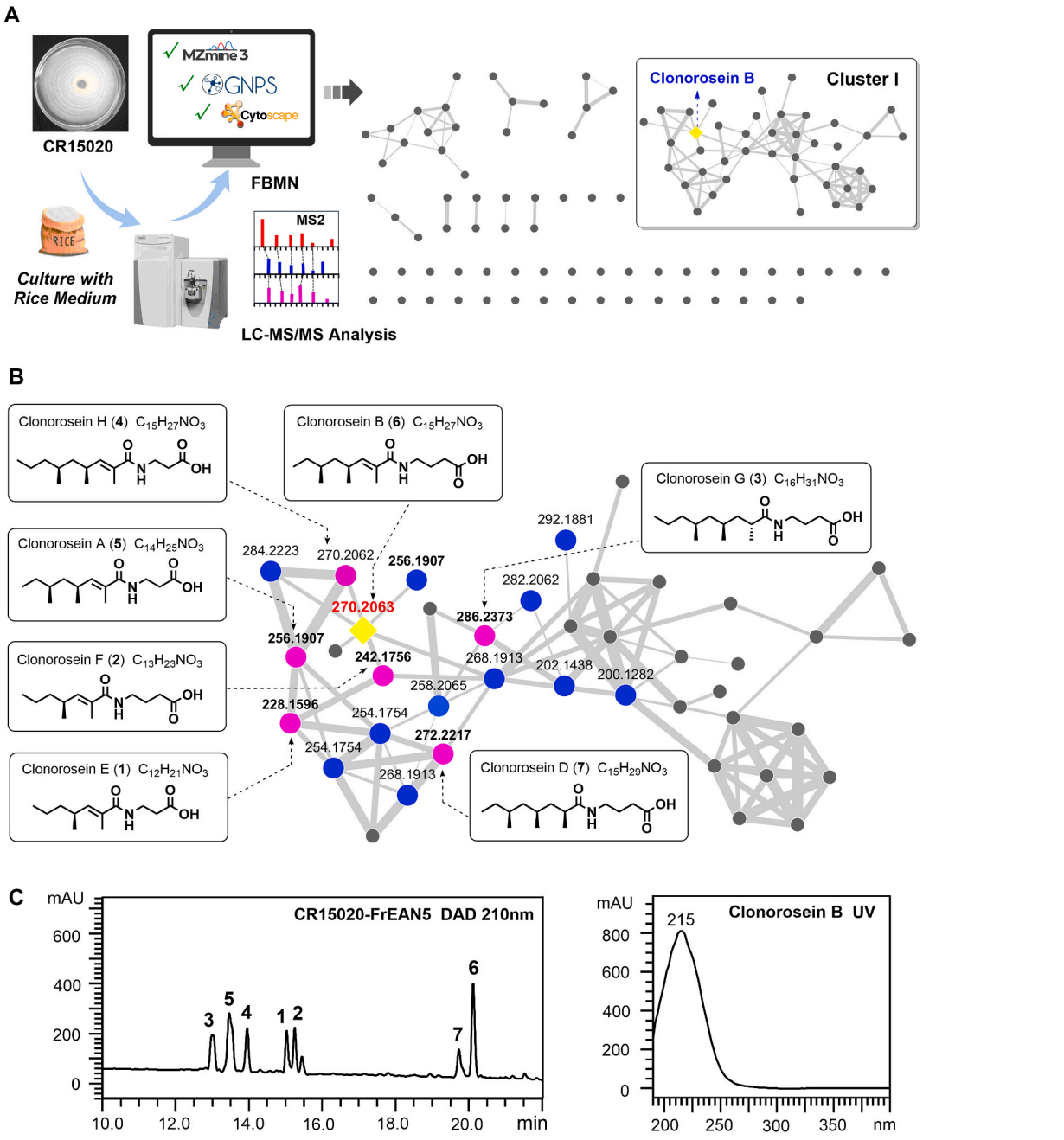

Fig. 2. FBMN-guided characterization of new clonorosein analogs. (A) Generation of feature-based molecular network (FBMN) of CR15020 crude extract cultured with rice medium, using Mzmine 3, GNPS and Cytoscape. (B) Clustering of clonorosein analogs. Clonorosein B was used as seed compound (yellow shaded square) in cluster analysis, and 17 clonorosein analogs (Purple circles: compounds isolated in this study; Blue circles: other potential new clonorosein analogs identified by HRMS annotation) were identified within the network. (C) HPLC-UV chromatogram of clonorosein fraction examined at 210 nm, and the UV spectrum of clonorosein B.

of two proton spin systems, including H-3–[H-4–H-11]–H-5–[H-6–H-12]–H-7–H-8–H-9, and NH–H-1′–H-2′. Further HMBC correlations of H_2-1′ to C-3′ and H_2-2′ to C-3′ indicated the presence of an N-substituted *β*-alanine moiety linked to an unsaturated acyl side chain through a 2-methyl-2-enamide group following the key HMBC correlations of H_3-10 to C-1, C-2, and C-3 and H_2-1′ to C-1. The *syn* configuration between C-2 and C-4 was revealed by comparing the Δδ of H-5a/H-5b with Hoplofungin A [26] and Amide 8b [27] (Fig. 3C), while further ECD calculation indicated that **4** preferred the 4*S*,6*R*-configuration (Fig. 4D). Thus, the structure of **4** was defined as outlined in Fig. 3A, and named clonorosein H.

The molecular formula of **7** was confirmed to be $C_{15}H_{29}O_3N$ based on HRESIMS (Fig. S8a) analysis (272.2220 $[M+H]^+$, calcd. for 272.2212), implying the presence of two degrees of unsaturation. The ^1H and ^{13}C NMR data of **7** (Table S1, Figs. S8b, S8c, and S8e) exhibited high similarity to those of **3**, with the exception of the elimination of one sp^3 methylene in the alkyl side chain. ^1H–^1H COSY crosspeaks uncovered the existence of two subunits, H-9–H-2–H-3–[H-4–H-10]–H-5–[H-6–H-11]–H-7–H-8, and NH–H-1′–H-2′–H-3′. The acyl side chain was verified to be 2,4,6-trimethyl-octanoyl according to critical HMBC correlations of H_3-9 to C-1/C-2/C-3, H_3-10 to C-3/C-4/C-5, H_3-11 to C-5/C-6/C-7, and H_3-8 to C-6/C-7 (Fig. S8d). The *syn* configuration between C-2 and C-4 was confirmed based on the large Δδ value between H-3a and H-3b (Δδ = 0.66 ppm) [25]. C-4 and C-6 were determined to be in a *syn*

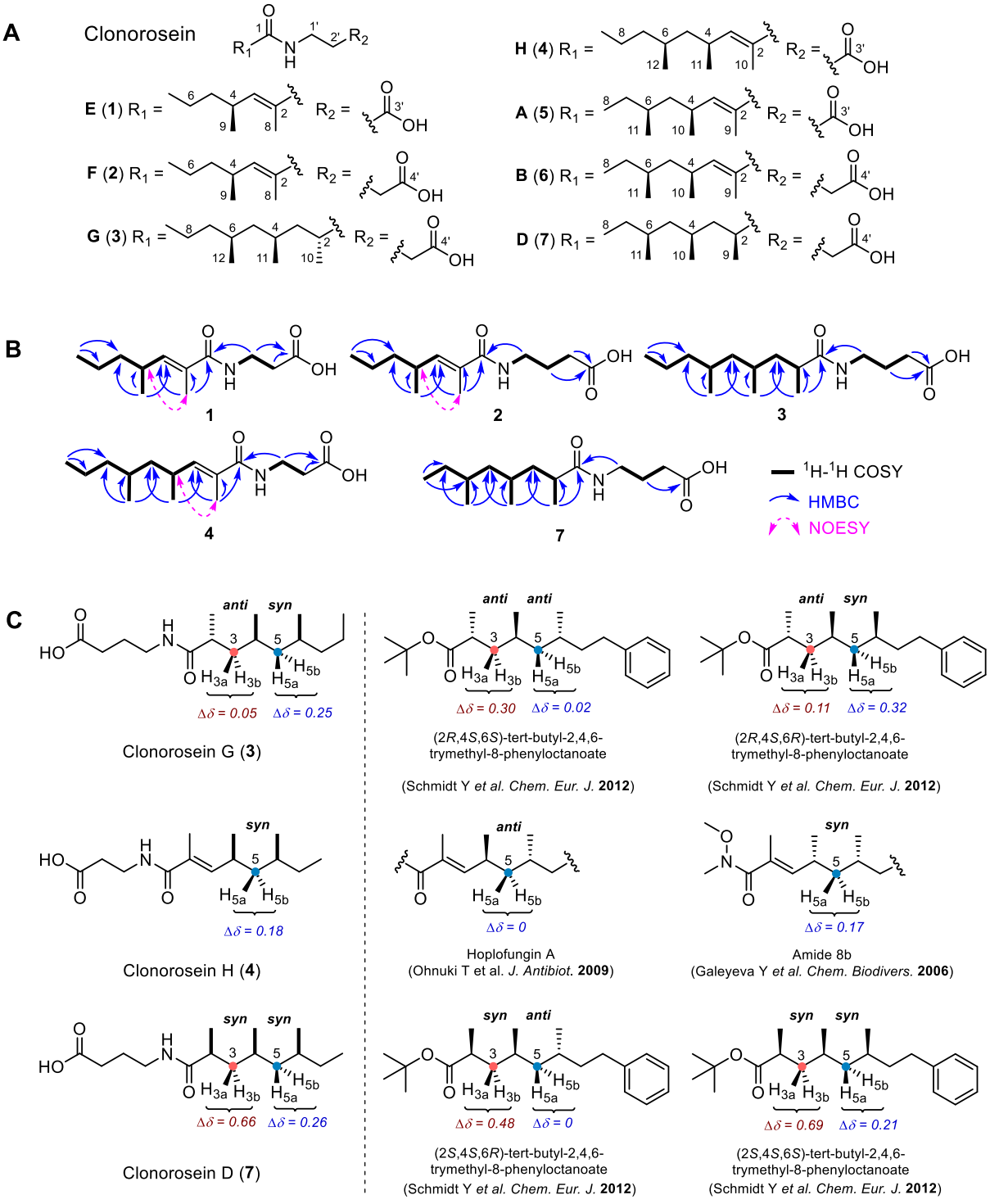

Fig. 3. Structure elucidation of clonoroseins and relative configuration determination. (A) Chemical structures of clonoroseins E–H (**1**–**4**), and clonoroseins A, B, and D (**5**–**7**). (B) 2D NMR correlations of clonoroseins E–H (**1**–**4**), and D (**7**). (C) Chemical-shift differences (Δδ) at H-3 and H-5 of clonoroseins G (**3**), H (**4**), D (**7**), and comparison to published data.

configuration via comparisons between the Δδ of H-3a/H-3b and H-5a/H-5b and the synthesized compounds (2*S*,4*S*,6*R*)-*tert*-butyl-2,4,6-trymethyl-8-phenyloctanoate and (2*S*,4*S*,6*S*)-*tert*-butyl-2,4,6-trymethyl-8-phenyloctanoate [25] (Fig. 3C). Further ECD determination revealed the absolute configuration of **7** to be 2*R*,4*R*,6*S*- (Fig. 4E). Therefore, the structure of **7** was identical to the identified compound clonorosein D [6], and its spectroscopic data and structural elucidation are presented in this study for the first time.

3.4. In vitro anti-microbial and cytotoxicity assay

As clonoroseins A and B inhibit the growth of the phytopathogens *Botrytis cinerea* and *Fusarium graminearum* at 64 μg/mL [6], we evaluated the antimicrobial activity of all seven isolated clonoroseins against human pathogens, such as *Staphylococcus aureus*, *Streptococcus mutans*, Methicillin-resistant *S. aureus*, *Streptococcus sanguis*, and *Candida albicans*, and several *Fusarium* sp. phytopathogens (Table S2). We also

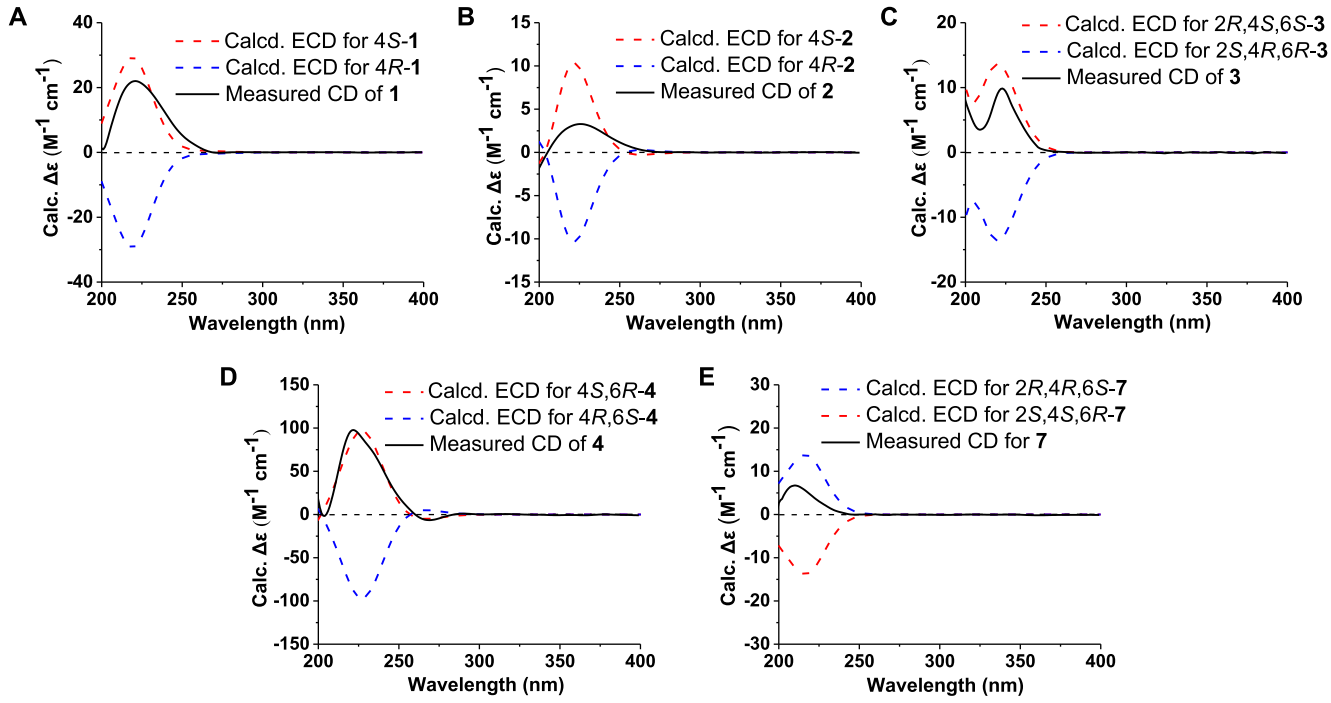

Fig. 4. Experimental CD and computed ECD of clonoroseins E–H (**1**–**4**), and D (**7**).

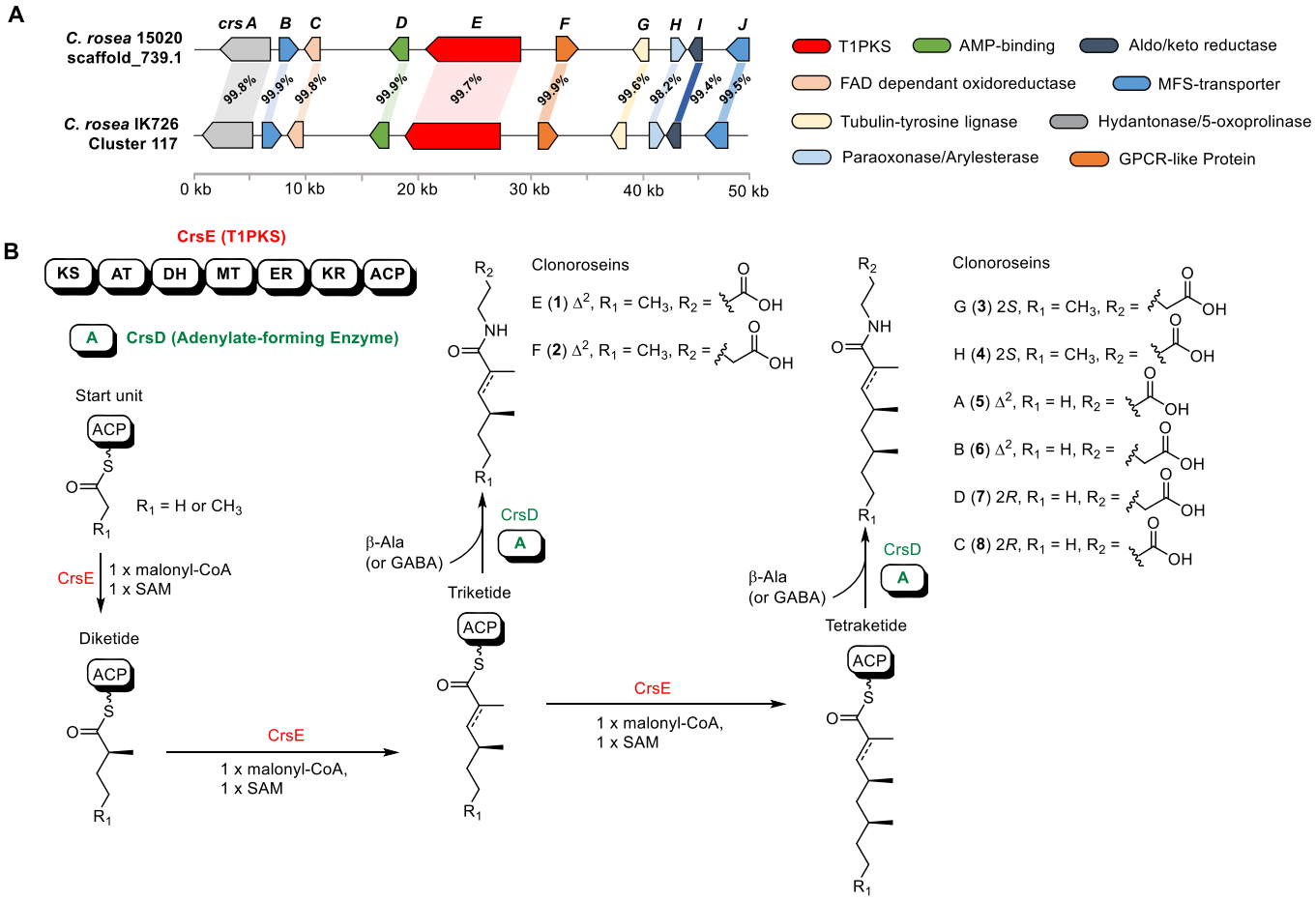

Fig. 5. Organization of the clonorosein biosynthetic gene cluster in CR15020 and *C. rosea* IK726 (A) and proposed biosynthetic pathway for isolated clonoroseins (B).

examined the cytotoxicity of these compounds against the HepG2 cell line (Table S3); however, no clear inhibitions could be observed at the concentration of 100 μg/mL in these assessments.

3.5. Proposed biosynthetic pathway of the isolated clonoroseins

To gain further information about clonorosein biosynthesis, we performed antiSMASH analysis on the CR15020 genome, revealing one candidate biosynthetic gene cluster (BGC) CR15020_scaffold739.1 (approximately 49.1 kb, accession no. ON817174), containing ten open reading frames (ORFs) (*crsA-crsJ*; Fig. 5A, Table 3) with a high sequence similarity to the genes in Cluster 117 of *C. rosea* IK726 [6]. CrsE showed 99.7 % identity with PKS22, which was responsible for the generation of acyl side chain in clonoroseins, testified by knockout experiment [6], while the enzyme responsible for the amide bond formation were still unknown.

The PKS gene (*crsE/pks22*) was flanked by putative 5-oxoprolinase (*crsA*), MFS-transporter (*crsB* and *crsJ*), FAD-dependent oxidoreductase (*crsC*), AMP-binding protein (*crsD*), GPCR-like protein (*crsF*), tubulin-tyrosine ligase (*crsG*), arylesterase (*crsH*), and aldo/keto reductase (CrsI) (Fig. 5A). The structures of clonoroseins are quite similar to fungal sourced *N*-acyl-amides wortmanamides (Hai and Tang 2018) generated by PKS-C enzyme, but unlike wortmanamides, thus hybrid enzymes like PKS-NRPS/PKS-C are not present in the *crs* cluster. BLASTP analysis utilizing the adenylate-forming protein (CrsD) as the query sequence in the Swiss-Prot database revealed CrsD was homologous to iboA (52 % similarity/31 % identity), which high likely activates the carboxylic acid to introduce an amide bond in the ibotenic acid biosynthesis [28].

We hypothesize that CrsD generate the acyl-AMP intermediates after the release of the polyketide side chain from PKS (CrsE), followed by the introduction of amide bonds through condensation with β-alanine (or γ-aminobutyric acid, GABA), generating the clonoroseins (Fig. 5B). Considering that polyketide chain length of clonoroseins varied among C_9 tetraketide (**3** and **4**), C_8 tetraketide (**5**−**7**), and C_7 triketide (**1** and **2**), the SAT domain of PKS (CrsE) may employ both acetyl-CoA and propionyl-CoA as beginning units (Fig. 5B), and a similar situation has been observed in AveAT0, the SAT domain of Avermectin PKS [29].

4. Discussion and conclusion

Plant endophytic fungi are important resources for new bioactive natural products discovery, while the capabilities of most species have not been uncovered yet [30]. Clonoroseins are a class of *N*-acylated aminoalkanoic acids first identified by Fatema et al. derived from the biocontrol agent *C. rosea* IK726, revealed by gene expression analysis during *C. rosea* interactions with the phytopathogens [6]. In this study, we characterized four new analogs, clonoroseins E−H (**1**−**4**), and discussed their biosynthesis for the first time.

N-acyl-amides or macrolactam from fungi are often generated by single-module PKS-NRPS [31] or PKS-C [32] hybrid enzymes. In the biosynthesis of wortmanamides, amide bonds between acyl units and β-alanine (or 5-aminopentanoic acid) are introduced by the C-domain in the PKS-C hybrid enzyme TwmB [32]. However, the clonorosein BGC only contains a single PKS gene (*crsE,* 99.7 % identity with *pks22*), and PKS-NRPS, PKS-C, or NRPS enzymes could not be identified. We proposed the adenylate-forming protein (CrsD) within *crs* cluster facilitates the transformation of the polyketide moiety into an acyl-AMP intermediate, followed by nucleophilic substitution with either β-alanine or γ-aminobutyric acid to generate clonoroseins. The ATP-dependent AMP-binding enzymes produce acyl-adenylate (acyl-AMP) which could be further substituted by different nucleophiles [33]. Several bacterial-derived AMP-binding enzymes were annotated as acyl-CoA synthetases but displayed catalytic functions related to the amination of acyl-AMP, including Ann1, Cfals, McbA, SimL, and AcsA [34–38]. The X-ray crystal structure of McbA displays a flexible C-terminal region, which undergoes a large rotation after acyl-adenylate formation to occlude the acyl binding pocket and generate the closed amino acid binding site [36]. To the best of our knowledge, fungal-derived adenylate-forming proteins with amination reactivity are rare reported, further functionality and catalytic mechanism study around this enzyme is undergoing.

Since clonoroseins A and B were reported to possess inhibition against *B. cinerea* and *F. graminearum at* 64 μg/mL [6], we also tested the antifungal activity of new clonoroseins E−H (**1**−**4**) obtained in this study against several phytopathogens belonging to *Fusarium* sp., while no obvious inhibition could be observed, partly due to the length and unsaturation degree of the polyketide side chain may influence the antifungal activity. Apart from this, NPs with similar structural features were found to possess interesting bioactivities. Bipolamides A&B are triene amides isolated from *Bipolaris* sp. MU34 is capable of inhibiting the growth of several filamentous fungi with a MIC of 16–64 μg/mL [39]. In addition, anandamide-like fatty acid amides could play a role as cannabinoid receptor ligands [40–42], while chlorinated fatty acid amides, known as columbamides exhibit potent biosurfactant action [43].

Over the past 5 years, molecular networking has been broadly utilized as an efficient mass data mining tool for new natural product discovery alongside MS-based metabolomics [44], and novel workflows, including FBMN [13], block-based molecular networking (BBMN) [45], and Ion Identity Molecular Networking (IIMN) [46]. It is believed that identifying gene clusters of molecular families will become attainable when MN can integrate genomic analysis [47].

In summary, a series of new *N*-acylated aminoalkanoic acids, called clonoroseins, were revealed from *C. rosea* CR15020 culture by applying FBMN. The possible biosynthetic pathway of clonoroseins has also been proposed according to BGC annotation. These results expand the limited knowledge of polyketide NPs produced by *C. rosea*, and provide an efficient method of determining and identifying new compounds using FBMN in the early stages of isolation.

CRediT authorship contribution statement

Jiaming Yu: Methodology, Investigation, Formal analysis,

Table 3
Deduced functions of ORFs in clonorosein (*crs*) BGC from CR15020 based on top BLASTP match.

Gene	Size (aa)	Proposed function	Origin of match	Accession no.	Identity (%)	Similarity (%)
crsA	1330	5-oxoprolinase	*Xylariales* sp. PMI_506	KAH8666815.1	76.75	87.51
crsB	520	Major facilitator superfamily protein	*Sarocladium implicatum*	KAH8171927.1	70.63	83.49
crsC	415	Sarcosine oxidase/l-pipecolate oxidase	*Geosmithia morbida*	XP_035324049.1	75.00	89.46
crsD	538	Adenylate-forming Enzyme	*Clonostachys rosea f. rosea IK726*	CAG9954636.1	99.44	99.81
crsE	2529	Highly reducing polyketide synthase g433	*Fusarium* sp.	A0A6S5ZY48.1	49.36	67.48
crsF	510	Unnamed protein product	*Clonostachys rhizophaga*	CAH0018916.1	90.46	91.91
crsG	474	tubulin-tyrosine ligase	*Colletotrichum plurivorum*	KAF6834567.1	67.43	81.95
crsH	390	Serum paraoxonase/arylesterase 1	*Tolypocladium ophioglossoides* CBS 100239	KND93492.1	53.59	71.79
crsI	338	putative aldo/keto reductase	*Talaromyces stipitatus* ATCC 10500	XP_002486045.1	67.76	82.51
crsJ	531	MFS general substrate transporter	*Aureobasidium pullulans* EXF-150	XP_029755998.1	74.63	85.32

Validation. **Yue Zhang:** Investigation, Validation, Formal analysis. **Li Zhang:** Investigation, Validation. **Jie Shi:** Investigation, Validation. **Kun Wang:** Investigation, Validation. **Weize Yuan:** Investigation, Validation. **Zexu Lin:** Investigation, Validation. **Shangqian Ning:** Investigation, Validation. **Bohao Wang:** Investigation, Validation. **Xinye Wang:** Investigation, Formal analysis. **Yuyang Qiu:** Investigation, Formal analysis. **Tom Hsiang:** Resources, Writing – review & editing. **Lixin Zhang:** Conceptualization, Resources, Writing – review & editing, Supervision. **Xueting Liu:** Conceptualization, Resources, Writing – review & editing, Supervision. **Guoliang Zhu:** Investigation, Formal analysis, Writing – original draft, Project administration.

Declaration of competing interest

Lixin Zhang is editor-in-chief for Synthetic and Systems Biotechnology and was not involved in the editorial review or the decision to publish this article. All authors declare that there are no competing interests.

Acknowledgement

We gratefully acknowledge financial support from the National Key Research and Development Program of China (2019YFA0906200), the National Natural Science Foundation of China (21977029, 81903529, 21877038, 31720103901, and 81573341), the Open Project Funding of the State Key Laboratory of Bioreactor Engineering, the 111 Project (B18022).

Appendix A. Supplementary data

Supplementary data to this article can be found online at https://doi.org/10.1016/j.synbio.2024.05.006.

References

[1] Newman DJ, Cragg GM. Natural products as sources of new drugs over the nearly four decades from 01/1981 to 09/2019. J Nat Prod 2020;83(3):770–803. https://doi.org/10.1021/acs.jnatprod.9b01285.
[2] Anjum R, Afzal M, Baber R, Khan M a J, Kanwal W, Sajid W, et al. Endophytes: as potential biocontrol agent-review and future prospects. J Agric Sci 2019;11(4):113–25. https://doi.org/10.5539/jas.v11n4p113.
[3] Romao-Dumaresq AS, Dourado MN, Favaro LC, Mendes R, Ferreira A, Araujo WL. Diversity of cultivated fungi associated with conventional and transgenic sugarcane and the interaction between endophytic *Trichoderma virens* and the host plant. PLoS One 2016;11(7):1–28. https://doi.org/10.1371/journal.pone.0158974.
[4] Sun ZB, Li SD, Ren Q, Xu JL, Lu X, Sun MH. Biology and applications of *Clonostachys rosea*. J Appl Microbiol 2020;129(3):486–95. https://doi.org/10.1111/jam.14625.
[5] Chatterton S, Punja ZK. Chitinase and β-1,3-glucanase enzyme production by the mycoparasite *Clonostachys rosea* f. *catenulata* against fungal plant pathogens. Can J Microbiol 2009;55(4):356–67. https://doi.org/10.1139/w08-156.
[6] Fatema U, Broberg A, Jensen DF, Karlsson M, Dubey M. Functional analysis of polyketide synthase genes in the biocontrol fungus *Clonostachys rosea*. Sci Rep 2018;8(1):15009. https://doi.org/10.1038/s41598-018-33391-1.
[7] Karlsson M, Durling MB, Choi J, Kosawang C, Lackner G, Tzelepis GD, et al. Insights on the evolution of mycoparasitism from the genome of *Clonostachys rosea*. Genome Biol Evol 2015;7(2):465–80. https://doi.org/10.1093/gbe/evu292.
[8] Sun ZB, Sun MH, Li SD. Draft genome sequence of mycoparasite *Clonostachys rosea* strain 67-1. Genome Announc 2015;3(3):1–2. https://doi.org/10.1128/genomeA.00546-15.
[9] Jin-Yan D, Hong-Ping H, Yue-Mao S, Zhang K-Q. Nematicidal epipolysulfanyldioxopiperazines from *Gliocladium roseum*. J Nat Prod 2005;68:1510–3. https://doi.org/10.1021/np0502241.
[10] Jiang CX, Yu B, Miao YM, Ren H, Xu Q, Zhao C, et al. Indole alkaloids from a soil-derived *Clonostachys rosea*. J Nat Prod 2021;84(9):2468–74. https://doi.org/10.1021/acs.jnatprod.1c00457.
[11] Zhai MM, Qi FM, Li J, Jiang CX, Hou Y, Shi YP, et al. Isolation of secondary metabolites from the soil-derived fungus *Clonostachys rosea* YRS-06, a biological control agent, and evaluation of antibacterial activity. J Agric Food Chem 2016;64(11):2298–306. https://doi.org/10.1021/acs.jafc.6b00556.
[12] Zhu G, Hou C, Yuan W, Wang Z, Zhang J, Jiang L, et al. Molecular networking assisted discovery and biosynthesis elucidation of the antimicrobial spiroketals epicospirocins. Chem Commun 2020;56(70):10171–4. https://doi.org/10.1039/d0cc03990j.
[13] Nothias LF, Petras D, Schmid R, Duhrkop K, Rainer J, Sarvepalli A, et al. Feature-based molecular networking in the GNPS analysis environment. Nat Methods 2020;17(9):905–8. https://doi.org/10.1038/s41592-020-0933-6.
[14] Rodrigues AMS, Lami R, Escoubeyrou K, Intertaglia L, Mazurek C, Doberva M, et al. Straightforward *N*-acyl homoserine lactone discovery and annotation by LC-MS/MS-based molecular networking. J Proteome Res 2022;21(3):635–42. https://doi.org/10.1021/acs.jproteome.1c00849.
[15] Xie HF, Kong YS, Li RZ, Nothias LF, Melnik AV, Zhang H, et al. Feature-based molecular networking analysis of the metabolites produced by in vitro solid-state fermentation reveals pathways for the bioconversion of epigallocatechin gallate. J Agric Food Chem 2020;68(30):7995–8007. https://doi.org/10.1021/acs.jafc.0c02983.
[16] Haridas S, Breuill C, Bohlmann J, Hsiang T. A biologist's guide to de novo genome assembly using next-generation sequence data: A test with fungal genomes. J Microbiol Methods 2011;86(3):368–75. https://doi.org/10.1016/j.mimet.2011.06.019.
[17] Larkin MA, Blackshields G, Brown NP, Chenna R, Mcgettigan PA, Mcwilliam H, et al. Clustal W and clustal X version 2.0. Bioinformatics 2007;23(21):2947–8. https://doi.org/10.1093/bioinformatics/btm404.
[18] Naruya S, Masatoshi N. The neighbor-joining method: a new method for reconstructing phylogenetic trees. Mol Biol Evol 1987;4(4):406–25. https://doi.org/10.1093/oxfordjournals/molbev/a040454.
[19] Kumar S, Stecher G, Tamura K. MEGA7: molecular evolutionary genetics analysis version 7.0 for bigger datasets. Mol Biol Evol 2016;33(7):1870–4. https://doi.org/10.1093/molbev/msw054.
[20] Frisch MJ, Trucks GW, Schlegel HB, Scuseria GE, Robb MA, Cheeseman JR, et al. Gaussian 09, revision A.02. Gaussian, Inc.; 2009.
[21] Cammi R, Tomasi J. Remarks on the use of the apparent surface charges (ASC) methods in solvation problems: iterative versus matrix-invrsion procedures and the renormalization of the apparent charges. J Comput Chem 1995;16(12):1449–58. https://doi.org/10.1002/jcc.540161202.
[22] Nalewajski RF. Density functional theory II. Berlin Heidelberg: Springer; 1996.
[23] Humphries RM, Ambler J, Mitchell SL, Castanheira M, Dingle T, Hindler JA, et al. CLSI methods development and standardization working group best practices for evaluation of antimicrobial susceptibility tests. J Clin Microbiol 2018;56(4):1–10. https://doi.org/10.1128/jcm.01934-17.
[24] Turkolmez S, Ozer G, Dervis S. Clonostachys rosea strain ST1140: an endophytic plant-growth-promoting fungus, and its potential use in seedbeds with wheat-grain substrate. Curr Microbiol 2022;80(1):36. https://doi.org/10.1007/s00284-022-03146-3.
[25] Schmidt Y, Lehr K, Colas L, Breit B. Assignment of relative configuration of desoxypropionates by ^{1}H NMR spectroscopy: method development, proof of principle by asymmetric total synthesis of xylarinic acid A and applications. Chemistry 2012;18(23):7071–81. https://doi.org/10.1002/chem.201103988.
[26] Ohnuki T, Yano T, Ono Y, Kozuma S, Suzuki T, Ogawa Y, et al. Haplofungins, novel inositol phosphorylceramide synthase inhibitors, from *Lauriomyces bellulus* SANK 26899 I. Taxonomy, fermentation, isolation and biological activities. J Antibiot (Tokyo) 2009;62(10):545–9. https://doi.org/10.1038/ja.2009.72.
[27] Yana G, Sarah H, Michael M, Florenz S, Manfred N, Sabine L, et al. Total synthesis and biological evaluation of (-)-Pectinatone employing a methyl-branched wax ester as key building block. Chem Biodivers 2006;3(8):935–41. https://doi.org/10.1002/cbdv.200690096.
[28] Obermaier S, Muller M. Ibotenic acid biosynthesis in the fly agaric is initiated by glutamate hydroxylation. Angew Chem Int Ed Engl 2020;59(30):12432–5. https://doi.org/10.1002/anie.202001870.
[29] Jiao YL, Wang LH, Jiao BH, Wang SJ, Fang YW, Liu S. Function analysis of a new type I PKS-SAT domain by Sat-Eat domain replacement. Appl Biochem Microbiol 2010;46(2):148–53. https://doi.org/10.1134/s0003683810020043.
[30] Elisashvili V. Submerged cultivation of medicinal mushrooms: bioprocesses and products. Int J Med Mushrooms 2012;14(3):211–39. https://doi.org/10.1615/intjmedmushr.v14.i3.10 (review).
[31] Zhang JM, Wang HH, Liu X, Hu CH, Zou Y. Heterologous and engineered biosynthesis of nematocidal polyketide-nonribosomal peptide hybrid macrolactone from extreme thermophilic fungi. J Am Chem Soc 2020;142(4):1957–65. https://doi.org/10.1021/jacs.9b11410.
[32] Hai Y, Tang Y. Biosynthesis of long-chain *N*-acyl amide by a truncated polyketide synthase-nonribosomal peptide synthetase hybrid megasynthase in fungi. J Am Chem Soc 2018;140(4):1271–4. https://doi.org/10.1021/jacs.7b13350.
[33] Schmelz S, Naismith JH. Adenylate-forming enzymes. Curr Opin Struct Biol 2009;19(6):666–71. https://doi.org/10.1016/j.sbi.2009.09.004.
[34] Abe T, Hashimoto Y, Sugimoto S, Kobayashi K, Kumano T, Kobayashi M. Amide compound synthesis by adenylation domain of bacillibactin synthetase. J Antibiot (Tokyo) 2017;70(4):435–42. https://doi.org/10.1038/ja.2016.117.
[35] Luft T, Li SM, Scheible H, Kammerer B, Heide L. Overexpression, purification and characterization of SimL, an amide synthetase involved in simocyclinone biosynthesis. Arch Microbiol 2005;183(4):277–85. https://doi.org/10.1007/s00203-005-0770-0.
[36] Petchey M, Cuetos A, Rowlinson B, Dannevald S, Frese A, Sutton PW, et al. The broad aryl acid specificity of the amide bond synthetase McbA suggests potential for the biocatalytic synthesis of amides. Angew Chem Int Ed Engl 2018;57(36):11584–8. https://doi.org/10.1002/anie.201804592.
[37] Winn M, Rowlinson M, Wang F, Bering L, Francis D, Levy C, et al. Discovery, characterization and engineering of ligases for amide synthesis. Nature 2021;593(7859):391–8. https://doi.org/10.1038/s41586-021-03447-w.

[38] Zhu J, Zhang S, Zechel DL, Paululat T, Bechthold A. Rational design of hybrid natural products by utilizing the promiscuity of an amide synthetase. ACS Chem Biol 2019;14(8):1793–801. https://doi.org/10.1021/acschembio.9b00351.
[39] Siriwach R, Kinoshita H, Kitani S, Igarashi Y, Pansuksan K, Panbangred W, et al. Bipolamides A and B, triene amides isolated from the endophytic fungus *Bipolaris* sp. MU34. J Antibiot (Tokyo) 2014;67(2):167–70. https://doi.org/10.1038/ja.2013.103.
[40] Bingnan H, Kerry LM, Alessia L, Vincenzo DM, Gerwick WH. Semiplenamides A-G, fatty acid amides from a Papua New Guinea collection. J Nat Prod 2003;66:1364–8. https://doi.org/10.1021/np030242n.
[41] Montaser R, Paul VJ, Luesch H. Marine cyanobacterial fatty acid amides acting on cannabinoid receptors. Chembiochem 2012;13(18):2676–81. https://doi.org/10.1002/cbic.201200502.
[42] William AD, Lumir H, Aviva B, Roger GP, Lesley AS, Graeme G, et al. Isolation and structure of a brain constituent that binds to the cannabinoid receptor. Science 1992;258(5090):1946–9. https://doi.org/10.1126/science.1470919.
[43] Mehjabin JJ, Wei L, Petitbois JG, Umezawa T, Matsuda F, Vairappan CS, et al. Biosurfactants from marine cyanobacteria collected in sabah, Malaysia. J Nat Prod 2020;83(6):1925–30. https://doi.org/10.1021/acs.jnatprod.0c00164.
[44] Jarmusch SA, Van Der Hooft JJJ, Dorrestein PC, Jarmusch AK. Advancements in capturing and mining mass spectrometry data are transforming natural products research. Nat Prod Rep 2021;38(11):2066–82. https://doi.org/10.1039/d1np00040c.
[45] He QF, Wu ZL, Li L, Sun WY, Wang GY, Jiang RW, et al. Discovery of neuritogenic securinega alkaloids from flueggea suffruticosa by a building blocks-based molecular network strategy. Angew Chem Int Ed Engl 2021;60(36):19609–13. https://doi.org/10.1002/anie.202103878.
[46] Schmid R, Petras D, Nothias LF, Wang M, Aron AT, Jagels A, et al. Ion identity molecular networking for mass spectrometry-based metabolomics in the GNPS environment. Nat Commun 2021;12(1):3832. https://doi.org/10.1038/s41467-021-23953-9.
[47] Quinn RA, Nothias LF, Vining O, Meehan M, Esquenazi E, Dorrestein PC. Molecular networking as a drug discovery, drug metabolism, and precision medicine strategy. Trends Pharmacol Sci 2017;38(2):143–54. https://doi.org/10.1016/j.tips.2016.10.011.